Investigation of the Cr:LiSrAlF$_6$ crystal by high-temperature Raman spectroscopy*

Wang Di(王 迪)[a], Wan Song-Ming(万松明)[a], Zhang Qing-Li(张庆礼)[a], Sun Dun-Lu(孙敦陆)[a], Gu Gui-Xin(顾桂新)[a], Yin Shao-Tang(殷绍唐)[a]†
Zhang Guo-Chun(张国春)[b], You Jing-Lin(尤静林)[c], and Wang Yuan-Yuan(王媛媛)[c]

[a] *Anhui Institute of Optics and Fine Mechanics, Chinese Academy of Sciences, Hefei* 230031, *China*
[b] *Technical Institute of Physics and Chemistry, Chinese Academy of Sciences, Beijing* 100190, *China*
[c] *Shanghai Enhanced Laboratory of Ferro-metallurgy, Shanghai University, Shanghai* 200072, *China*

(Received 17 January 2011; revised manuscript received 27 May 2011)

In this paper, Cr-doped LiSrAlF$_6$ crystals are investigated using high-temperature Raman spectroscopy and the single-crystal Raman spectra of Cr:LiSrAlF$_6$ are analysed by factor group theory and comparison with other fluorides. The results indicate that Cr:LiSrAlF$_6$ is stable below its melting point; Raman peaks located at 561, 322 and 250 cm^{-1} are assigned to the A_{1g} modes of AlF$_6$, SrF$_6$ and LiF$_6$ octachdra, respectively; with temperature increasing, Raman peaks associated with AlF$_6$ octahedra shift towards low frequencies, while LiF$_6$ and SrF$_6$ octahedra are temperature-insensitive; around the crystal melting point, three new Raman peaks occur, which are associated with the AlF$_6$ octahedral chain structure. Finally, the microstructural evolution of Cr:LiSrAlF$_6$ from room temperature to its melting point is discussed based on its Raman spectra.

Keywords: Cr:LiSrAlF$_6$ crystal, high-temperature Raman spectroscopy, crystal structure, *in situ* investigation

PACS: 81.10.–h, 36.20.Ng, 42.70.Hj **DOI:** 10.1088/1674-1056/20/10/108101

1. Introduction

Cr-doped LiSrAlF$_6$ (LSAF) or LiCaAlF$_6$ (LCAF) crystals are considered as promising materials for use in low-cost, single-mode diode-pumped lasers.[1–6] They have the capability of being effectively pumped directly by diode lasers and also have a broad tuning range with the possibility of having a narrow laser line width, which make them a potential alternative to Ti:Sapphire.[2] Since high quality Cr-doped LSAF or LCAF crystals for laser applications are hard to grow, many researchers have focused on crystal growth technology.[7–9] Nevertheless, the crystal growth mechanisms of Cr-doped LSAF or LCAF crystals and the dynamic processes of crystal growth at a molecular level are still not clear.

In our previous studies, the growth mechanisms of various oxide crystals were studied using high-temperature Raman spectroscopy.[10,11] The results indicated that the microstructural evolution of crystals at high temperature is essential for the study of crystal growth mechanisms and for the interpretation of crystal growth habits. However, these studies all focus on the growth mechanisms of oxide crystals, non-oxide crystals have not yet been considered. In order to extend our knowledge about crystal growth mechanisms, it is important and necessary to study non-oxide crystals such as Cr-doped LSAF or LCAF.

With advantages of *in situ* observation, microscale analysis and high-temperature measurement, high-temperature Raman spectroscopy is a suitable tool to study the microstructural evolution of a material at high temperature.[12] Wan *et al.*[13,14] investigated the microstructure of the melt-crystal interface of borate crystals using high-temperature Raman spectroscopy and discussed crystal growth habits. In the present work, the single-crystal Raman spectra of Cr:LSAF from room temperature to its melting point (1063 K) are obtained by using high-temperature Raman spectroscopy. Based on the single-crystal Raman spectrum of LCAF[15] and high-temperature X-ray diffraction data of LSAF,[16,17] the microstructural evolution of Cr:LSAF from room temperature to its melting point is discussed.

*Project supported by the Key Program of the National Natural Science Foundation of China (Grant No. 50932005) and the Open Poject of Shanghai Key Laboratory of Modern Metallurgy and Materials Processing (Grant No. SELF-2009-01).
†Corresponding author. E-mail: shtyin@aiofm.ac.cn
© 2011 Chinese Physical Society and IOP Publishing Ltd

2. Experimental details

The Cr:LSAF single crystal was grown by the Czochralski method.[18] It was cut into slices each with a size of Φ4.5 mm×2 mm and theses slices were placed in a platinum crucible. The crucible was heated from room temperature to the crystal melting point (1063 K) at a heating rate of 10 K/min using a Leitz Microscopy Heating Stage 1350. During the heating process, Cr:LSAF was protected by high pure Ar gas to avoid oxidation of the crystal at high temperature.

Room and high-temperature Raman spectra were obtained using a Jobin Y'von U1000 laser Raman spectrometer. The pulsed exciting light (355 nm) from a Q-switch pulsed THG-Nd:YAG laser was focused on Cr:LSAF by an Olympus BH-2 microscope and Raman scattering light from the crystal was collected by a back-scattering confocal lens system and detected by an intensive charge-coupled device (ICCD). All spectra were recorded in a range of 200 cm^{-1}–800 cm^{-1} with a spectral resolution of 1 cm^{-1}. The experiment system is shown in Fig. 1.

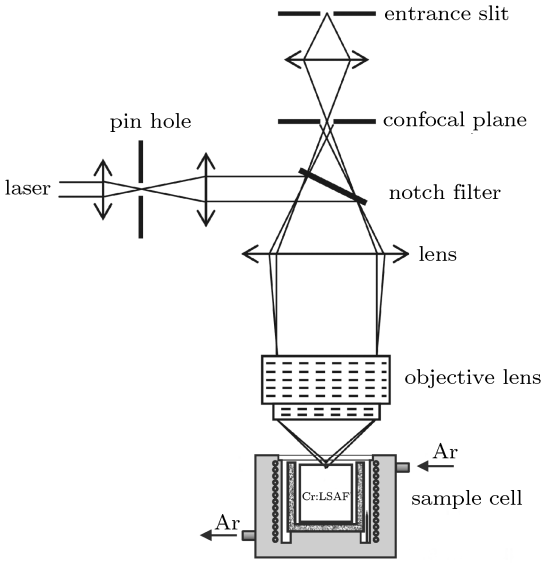


Fig. 1. Schematic diagram of the experimental system.

3. Results and discussion

3.1. Room-temperature Raman spectrum

The crystal structure of LSAF has trigonal symmetry with the space group $P\bar{3}1c$. Li^+ and Al^{3+} occupy the D_3 site, Sr^{2+} occupies the S_6 site and F^-occupies the C_1 site. Each cation occupies the central sites of a deformed fluoride octahedron, all these octahedra form successive alternate layers along the c axis, the AlF_6 and the LiF_6 octahedra exist in the same layers and link together with each other to form hexagonal rings by sharing edges, the SrF_6 octahedra exist separately in another layer and share corner F^- ions with the AlF_6 and LiF_6 octahedra[19] as shown in Fig. 2.

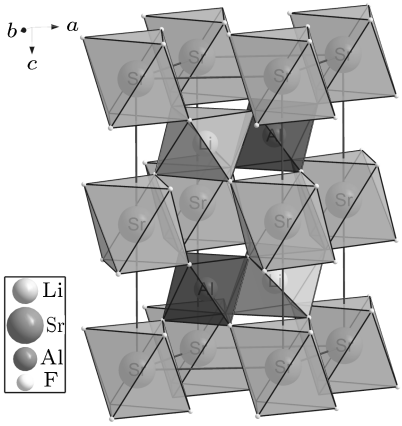


Fig. 2. Crystal structure of LSAF.

Due to the structural similarity, factor group analysis predicts that there is no difference in Raman vibrational mode between LSAF and LCAF, i.e., 36 optical normal modes, $3A_{1g}+8E_g$ of which is Raman active-mode. Three A_{1g} modes are ascribed to the breathing modes of F^- ions in an octahedron and the E_g mode is ascribed to the distortion of the fluorine octahedron or motion of Li^+ and Al^{3+} ions.

$$\Gamma_{\rm Al} = A_{2g} + A_{2u} + E_g^* + E_u,$$
$$\Gamma_{\rm Li} = A_{2g} + A_{2u} + E_g^* + E_u,$$
$$\Gamma_{\rm Sr} = A_{1u} + A_{2u} + 2E_u,$$
$$\Gamma_{\rm F} = 3A_{1g}^* + 3A_{1u} + 3A_{2g} + 3A_{2u} + 6E_g^* + 6E_u,$$
$$\Gamma_{\rm LSAF} = 3A_{1g}^* + 8E_g^* + 5A_{2g} + 6A_{2u} + 10E_u + 4A_{1u}.$$

* : Raman active mode.

Kontos *et al.*[20] compared the room-temperature Raman spectrum of Cr-doped LSAF crystal with that of the pure LSAF crystal. The results indicated that the single-crystal Raman spectrum of LSAF was not affected by Cr ion doping, so the influence of Cr ions on Raman spectra is reasonably neglected in this work.

Figure 3 shows the room-temperature Raman spectrum of Cr:LSAF in a range from 200 cm^{-1} to 800 cm^{-1}. Only seven Raman peaks are found, which are located at 232, 250, 322, 376, 408, 436, and 561 cm^{-1}, respectively. Since assignations of Raman peaks have not been completely clear until now, a fur-

ther assignation of Cr:LSAF will be given by comparison with other fluorides in this work.

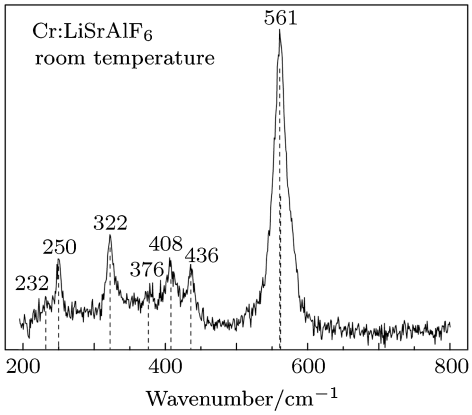


Fig. 3. Room-temperature Raman spectrum of Cr:LSAF.

Boulard *et al.*[21] studied the relationship between the symmetric stretching frequencies of the A_{1g} mode and the structure of a fluoride octahedron in detail. The results indicated that if the connectivity degree of two fluoride octahedra is similar, A_{1g} mode frequencies of two octahedra have the following relationship:

$$\omega_{A_{1g}}\left(\mathrm{cm}^{-1}\right) = \omega'_{A_{1g}}\left(\mathrm{cm}^{-1}\right)\left(\frac{r'}{r}\right)^{3/2}\left(\frac{Z_M}{Z'_M}\right)^{1/2}, \quad (1)$$

where r and r' are the metal-fluorine bond length, Z_M and Z'_M are the electric charge of the metal ions respectively. Based on formula (1) and A_{1g} mode frequencies of fluorides (LCAF,[15] CoF_2,[21] and MnF_2[21]), A_{1g} mode frequencies of Cr:LSAF are calculated and presented in Table 1. Using Raman and structural data of LCAF, three calculated A_{1g} modes of Cr:LSAF are 561, 334.7, and 279.7 cm^{-1}, for AlF_6, SrF_6, and LiF_6 octahedra. Using the experimental data of CoF_2 and MnF_2, the calculated A_{1g} modes of AlF_6 and LiF_6 octahedra are 549.3 cm^{-1} and 268.1 cm^{-1}, 530.1 cm^{-1}, and 258.7 cm^{-1}. These calculated results are very close to three Raman peaks of Cr:LSAF at 561, 322, and 250 cm^{-1}, which should be related to A_{1g} modes of AlF_6, SrF_6 and LiF_6 octahedra, respectively.

Among 11 Raman-active modes of Cr:LSAF, four vibrational modes (A_{1g}+3E_g) belong to Al–F_6 octahedra. Vibrations of AlF_6 octahedra are independent due to strong interactions of Al–F bonds, therefore, Raman peaks associated with the AlF_6 octahedron of Cr:LSAF should be similar to those of LCAF. Three Raman peaks of Cr:LSAF, which are located at 561, 436, and 408 cm^{-1}, are very close to the A_{1g} mode (564 cm^{-1}) and two E_g modes (436 cm^{-1} and 412 cm^{-1}) of LCAF.[15] This comparison implies that the A_{1g} mode of Cr:LSAF is consistent with the above calculated result, two Raman peaks of Cr:LSAF at 436 cm^{-1} and 408 cm^{-1} are ascribed to E_g mode of AlF_6 octahedron, while the third one is not confirmed.

Table 1. Calculated frequencies of the A_{1g} modes of Cr:LSAF* crystal.

Fluoride crystals	Experimental Results frequency/cm^{-1}	M–F/Å	Calculated frequencies (cm^{-1}) of Cr:LSAF		
			ω_{Al-F}	ω_{Sr-F}	ω_{Li-F}
CoF_2	$364_{(Co-F)}$	$2.076_{(Co-F)}$	549.3		268.1
MnF_2	$338_{(Mn-F)}$	$2.130_{(Mn-F)}$	530.1		258.7
LCAF	$562_{(Al-F)}$	$1.8055_{(Al-F)}$	561.7		
	$368_{(Ca-F)}$	$2.2807_{(Ca-F)}$		334.7	
	$282_{(Li-F)}$	$2.0095_{(Li-F)}$			279.7

*: Al–F bondlength of LSAF[16] is 1.8062 Å, Li–F 2.0205 Å, Sr–F 2.4294 Å (1 Å=0.1 nm).

3.2. High-temperature Raman spectra

Figure 4 shows high-temperature Raman spectra of Cr:LSAF from 473 K to its melting point. With temperature increasing, the intensity of the Raman spectrum decreases, Raman peaks broaden and shift toward lower frequencies due to thermal disturbance and crystal lattice swelling. The temperature dependencies of the Raman peaks associated with different octahedra are different, the temperature coefficient ($\mathrm{d}\omega/\mathrm{d}T$) can reflect the thermal properties of Cr:LSAF. Figure 5 shows the temperature dependencies of the Raman peaks located at 561 cm^{-1} and 250 cm^{-1}. A linear relationship between peak frequency and heating temperature is found. The temperature coefficients of the Raman peaks of Cr:LSAF are obtained and listed in Table 2. It can be found that the temperature coefficients of Raman peaks (561, 436, and 408 cm^{-1}) related to the AlF_6 octahedron are larger than those of Raman peaks (322 cm^{-1} and 250 cm^{-1}) related to SrF_6 and LiF_6 octahedra, which

indicates that the AlF_6 octahedron is more sensitive to high temperature than SrF_6 and LiF_6 octahedra in Cr:LSAF.

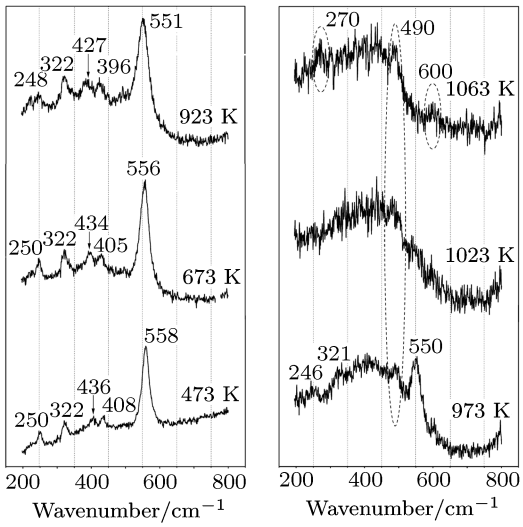


Fig. 4. High-temperature Raman spectra of the Cr:LSAF crystal from 473 to 1063 K.

Cr:LSAF has a highly negative thermal expansion along the c axis.[16] Grzechnik *et al.*[17] studied crystal structures of LSAF at different temperatures using high resolution X-ray diffraction (XRD). The results indicated that with temperature increasing, the interatomic distances of the Al–F bond in the AlF_6–LiF_6 layers and F–F bond in the SrF_6 layers decrease. According to formula (1), the decrease of the Al–F bond should cause the A_{1g} mode of AlF_6 octahedron to be "blue shifted", which seems to be conflict with "red shift" in this work. Boulard *et al.*[21] also suggested that the frequency of the A_{1g} mode decreased with the degree of octahedron connectivity increasing. Xiao *et al.*[22] studied Raman spectra of an alkali fluoroaluminate system using *ab initio* calculation and found that the calculated Raman frequency was close to experimental data based on supermolecule clusters. On the basis of their work, the "red shift" of the A_{1g} mode reflects the enhancement of the interaction among AlF_6 octahedra in Cr:LSAF.

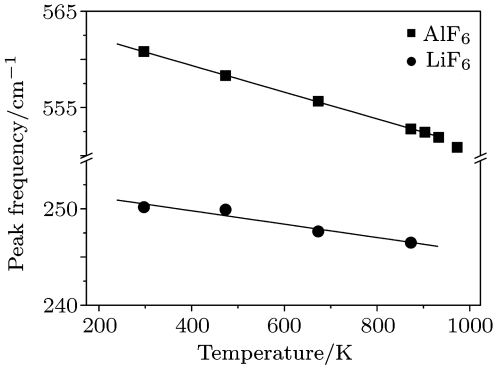


Fig. 5. Temperature dependencies of A_{1g} modes of AlF_6 and LiF_6 octahedra.

Table 2. Temperature coefficients of Raman peaks.

Raman peak/cm^{-1}	561	436	408	322	250
$d\omega/dT$	–0.014	–0.024	–0.033	–0.003	–0.007

When temperature is above 973 K, the Raman peaks of Cr:LSAF vanish except for the A_{1g} mode of the AlF_6 octahedron at 550 cm^{-1}, a broad Raman band appears in a range from 200 cm^{-1} to 600 cm^{-1} (see Fig. 4), which is attributed to the bending and symmetric stretching vibrations of nonbridging fluorine atoms.[23,24] These changes of Raman spectra indicate that many octahedra become unstable at this temperature expect for the AlF_6 octahedron. Around the crystal melting point, the Raman peak at 550 cm^{-1} disappears, which is accompanied with three new Raman peaks appearing at 270, 490, and 600 cm^{-1}. The similar Raman peaks are observed in $SrAlF_5$ crystal,[25] of which three characteristic vibrational peaks are located at 290, 515, and 600 cm^{-1}. It is well known that in the $SrAlF_5$ crystal, the AlF_6 octahedron forms a chain structure by sharing the apical F^- ions along the c axis, Sr^{2+} ions are distributed in the fluoroaluminate frame.[26] Therefore, the Raman spectrum indicates that the discrete AlF_6 octahedra of Cr:LSAF transforms into the AlF_6 octahedron chain structure around the crystal melting point.

According to the above analysis, the microstructural evolution of Cr:LSAF from room temperature to its melting point is proposed as shown in Fig. 6. With the increase of temperature, the decreasing of F–Sr–F angle and twist angle of SrF_6 octahedra causes the F–F bonds to contract along the c axis, which makes the upper and lower AlF_6 octahedra gradually approach each other.[16,17] Around the crystal melting point, the deformed LiF_6 and SrF_6 octahedra become unstable and damaged, and then the approaching AlF_6 octahedra connect with each other and form AlF_6 octahedra

chain structures.

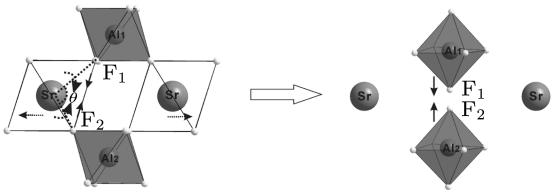


Fig. 6. Distortions of octahedra in the Cr:LSAF crystal. The closed face octahedra are AlF_6 units, the open face octahedra are SrF_6 units. F_1 is the fluorine atom shared by the SrF_6 octahedron with the upper AlF_6 octahedron. F_2 is the fluorine atom shared by the SrF_6 octahedron with the lower AlF_6 octahedron. θ is the F_1–Sr–F_2 angle.

4. Conclusion

In conclusion, Raman spectra of Cr:LSAF are obtained using high-temperature Raman spectroscopy. Analysis of the room-temperature spectrum indicates that Raman peaks at 561, 322, and 250 cm^{-1} are assigned to A_{1g} modes of AlF_6, SrF_6, and LiF_6 octachdra, respectively. High-temperature Raman spectra indicate that the crystal structure is stable below its melting point; with temperature increasing, Raman peaks of Cr:LSAF shift towards lower frequencies by different degrees; around the crystal melting point, three new Raman peaks associated with AlF_6 octahedron chain structures come into being. Based on the Raman spectra, microstructural evolution of Cr:LSAF from room temperature to its melting point is discussed.

References

[1] Majkić A, Poberaj G, Degl'Innocenti R, Döbeli M and Günter P 2007 *Appl. Phys.* B **88** 205

[2] Demirbas U, Li D, Birge J R, Sennaroglu A, Petrich G S, Kolodziejski L A, Kärtner F X and Fujimoto J G 2009 *Opt. Express* **17** 14374

[3] Demirbas U, Sennaroglu A, Benedick A, Siddiqui A, Kärtner F X and Fujimoto J G 2007 *Opt. Lett.* **32** 3309

[4] Demirbas U, Sennaroglu A, Kärtner F X and Fujimoto J G 2009 *J. Opt. Soc. Am.* B **26** 64

[5] Prasankumar R, Hirakawa Y, Kowalevicz Jr A, Kärtner F, Fujimoto J and Knox W 2003 *Opt. Express* **11** 1265

[6] Demirbas U, Sennaroglu A, Kärtner F X and Fujimoto J G 2008 *Opt. Lett.* **33** 590

[7] Castillo V K and Quarles G J 1997 *J. Cryst. Growth* **174** 337

[8] Klimm D, Lacayo G and Reiche P 2000 *J. Cryst. Growth* **210** 683

[9] Sato H, Machidab H, Nikl M, Yoshikawaa A and Fukuda T 2003 *J. Cryst. Growth* **250** 83

[10] Zhou W P, Wan S M, Yin S T, Zhang Q L, You J L and Wang Y Y 2009 *Acta Phys. Sin.* **58** 570 (in Chinese)

[11] Zhou W P, Wan S M, Zhang X, Zhang Q L, You J L, Qiu H L and Yin S T 2008 *Acta Phys. Sin.* **57** 7305 (in Chinese)

[12] You J L, Jiang G C, Yang S H, Ma J C and Xu K D 2001 *Chin. Phys. Lett.* **18** 991

[13] Wan S M, Zhang X, Zhao S J, Zhang Q L, You J L, Chen H, Zhang G C and Yin S T 2007 *J. Appl. Crystallogr.* **40** 725

[14] Wan S M, Zhang X, Zhao S J, Zhang Q L, You J L, Lu L, Fu P Z and Wu Y C 2008 *Cryst. Growth Des.* **8** 412

[15] Daniel P, Gesland J Y and Roussean M 1992 *J. Raman Spectrosc.* **23** 197

[16] Kuze S, Boulay D D, Ishizawa N, Kodama N, Yamaga M and Hendersone B 2004 *J. Solid State Chem.* **177** 3505

[17] Grzechnik A, Dmitriev V, Weber H P, Gesland J Y and Friese K 2004 *J. Phys.: Condens. Matter* **16** 5769

[18] Zhang S G, Han Q Y, Hu W D and Tao D J 1995 *Chin. J. Quantum Electron.* **12** 236 (in Chinese)

[19] Schaffers K I and Keszler D A 1991 *Acta Crystallographica* C **47** 18

[20] Kontos A G, Tsaknakis G, Raptis Y S, Papayannis A, Landulfo E, Baldochi S L, Barbosa E and Viera N D 2003 *J. Appl. Phys.* **93** 2797

[21] Boulard B, Jacoboni C and Rousseau M 1989 *J. Solid State Chem.* **80** 17

[22] Xiao L, You J L and Jiang G C 2008 *Chin. J. Nonferrous Met.* **18** 1164 (in Chinese)

[23] Papatheodorou G N and Dracopoulos V 1995 *Chem. Phys. Lett.* **241** 345

[24] Almeida R M, Pereira J C, Messaddeq Y and Aegerter M A 1993 *J. Non-Cryst. Solids* **161** 105

[25] Silva E N, Ayala A P, Filho M J, Moreira R L and Gesland J Y 2004 *J. Phys.: Condens. Matter* **16** 7511

[26] Frank K 1998 *Z. Anorg. Allg. Chem.* **624** 1481